HHS Public Access

Author manuscript

Mol Imaging Biol. Author manuscript; available in PMC 2021 December 01.

Published in final edited form as:

Mol Imaging Biol. 2020 December ; 22(6): 1532–1542. doi:10.1007/s11307-020-01524-6.

Preclinical assessment of the effectiveness of magnetic resonance molecular imaging of extradomain-B fibronectin for detection and characterization of oral cancer

Ryan C. Hall[1], **Nadia R. Ayat**[1], **Peter L. Qiao**[1], **Amita M. Vaidya**[1], **Dan Ma**[1], **Anita Aminoshariae**[2], **Ivan Stojanov**[3,4], **Zheng-Rong Lu**[1,5]

[1]Department of Biomedical Engineering, Case Western Reserve University, Cleveland, Ohio 44106, USA

[2]Department of Endodontics, Case Western Reserve University, Cleveland, Ohio 44106, USA

[3]Department of Oral and Maxillofacial Medicine and Diagnostic Sciences, Case Western Reserve University, Cleveland, Ohio 44106, USA

[4]Department of Pathology, Case Western Reserve University, Cleveland, Ohio 44106, USA

[5]Case Comprehensive Cancer Center, Case Western Reserve University, Cleveland, Ohio 44106, USA

Abstract

Purpose—Oral squamous cell carcinoma (OSCC) has not seen a substantial improvement in patient survival despite therapeutic advances, making accurate detection and characterization of the disease a clinical priority. Here, we aim to demonstrate the effectiveness of magnetic resonance imaging (MRI) with the targeted MRI contrast agent MT218 specific to extradomain-B fibronectin (EDB-FN) in the tumor microenvironment for detection and characterization of aggressive OSCC tumors.

Procedures—EDB-FN expression was evaluated in human normal tongue and OSCC specimens with immunohistochemistry. Invasiveness of human CAL27, HSC3, and SCC4 OSCC cells was analyzed with spheroid formation and Transwell assays. EDB-FN expression in the cells was analyzed with semi-quantitative real-time PCR, western blotting, and a peptide binding study with

*To whom correspondence should be addressed: Dr. Zheng-Rong Lu, Wickenden 427, Mail Stop 7207, 10900 Euclid Avenue, Cleveland, OH 44106, Phone: 216-368-0187, Fax: 216-368-4969, zxl125@case.edu.

Author Contributions

Conceptual design of the research was coordinated by ZRL and RCH. All aspects of experimental execution were done by RCH. NRA and PLQ contributed to MRI data acquisition. NRA and AMV contributed to *in vitro* and *in vivo* data interpretation. IS reviewed all histological slides. AA assisted on clinical aspects of oral cancer, and DM assisted regarding MRI technique. The manuscript was prepared by RCH and ZRL and critically reviewed by NRA, PLQ, AMV, DM, AA, and IS.

Conflict of Interest Statement

ZRL is a co-founder of Molecular Theranostics, LLC, which is focused on the commercialization of targeted MRI contrast agents.

confocal microscopy. Contrast-enhanced MRI with MT218 was performed on subcutaneous OSCC mouse models at a dose of 0.04 mmol/kg, using gadoteridol (0.1 mmol/kg) as a control.

Results—Strong EDB-FN expression was observed in human untreated primary and metastatic OSCC, reduced expression in treated OSCC, and little expression in normal tongue tissue. SCC4 and HSC3 cell lines demonstrated high invasive potential with high and moderate EDB-FN expression, respectively, while CAL27 showed little invasive potential and low EDB-FN expression. In T_1-weighted MRI, MT218 produced differential contrast enhancement in the subcutaneous tumor models in correlation with EDB-FN expression in the cancer cells. Enhancement in the high-EDB-FN tumors was greater with MT218 at 0.04 mmol/kg than gadoteridol at 0.1 mmol/kg.

Conclusions—The results suggest EDB-FN has strong potential as an imageable biomarker for aggressive OSCC. MRMI results demonstrate the effectiveness of MT218 and the potential for differential diagnostic imaging of oral cancer for improving the management of the disease.

Keywords

MRMI; targeted contrast agent; extradomain-B fibronectin; oral squamous cell carcinoma; oral cancer; extracellular matrix; tumor microenvironment; cancer detection; risk stratification

Introduction

Oral squamous cell carcinoma (OSCC) is the most common malignant neoplasm of the oral cavity, representing more than 90% of oral malignancies [1]. Despite improvements in therapeutic options, the 5-year survival rate of OSCC patients remains just above 50% with little improvement [2]. This poor prognosis stems from late stage diagnosis, local invasion and metastasis, recurrence post-resection, and lack of targetable biomarkers for early and accurate detection [3]. Over 60% of patients are diagnosed with late-stage tumors, whose overall survival rate plummets to as low as 20% [4]. Conventional histological grading schemes do not reliably predict patient outcomes, necessitating the development of enhanced OSCC diagnostic methods to improve clinical outcomes [5].

Routine work-up for OSCC patients includes physical examination and diagnostic imaging to better delineate disease margins. Most patients have locally or regionally aggressive disease that is difficult to diagnose, and micrometastases to local lymph nodes highly correlate with adverse outcomes [4,6–7]. While the oral cavity can be physically examined, routine examinations do not consistently identify all biologically relevant precursor lesions, and adjuvant screening techniques lack the appropriate sensitivity and specificity to justify widespread use [8]. Common diagnostic imaging methods for OSCC include computed tomography (CT) and magnetic resonance imaging (MRI). Although both provide valuable diagnostic information, MRI offers superior soft tissue contrast, enabling more precise delineation of primary tumor boundaries, local invasion, and detection of metastases [9–11]. Consequently, MRI is often used to plan the scope of surgical resection, subsequent tissue reconstruction, and treatment monitoring for therapeutic efficacy and recurrence [9]. The most commonly used MRI contrast agents are gadolinium-based contrast agents (GBCAs) [12]. However, current GBCAs are untargeted, providing non-specific contrast enhancement

with no ability for disease characterization [12]. There is therefore an unmet clinical need to develop targeted GBCAs that enable precision imaging of OSCC for accurate detection, delineation, and characterization to enhance diagnosis and guide timely precision treatment.

Tumor extracellular matrix (ECM) proteins closely interact with tumor cells and mediate many biological processes associated with tumor progression [13]. Upregulated ECM fibronectin is associated with tumor invasion, metastasis, and therapy resistance [14]. Extradomain-B fibronectin (EDB-FN), a fibronectin splice-variant involved in neovascularization, is also upregulated in many aggressive cancers, including pancreatic, breast, and oral cancers, with little expression in normal adult tissues [14]. The presence of EDB-FN in epithelial tumor cells indicates their inherent ability to produce the protein in conjunction with EDB-FN produced by stromal cells [15–18]. Recent studies show differential expression of EDB-FN in prostate and breast cancers positively correlating with tumor aggressiveness [15–16,19–21]. In OSCC, EDB-FN exhibits variable expression in upwards of 100% of primary tumors and 96% of cervical metastases, suggesting its potential for diagnostic imaging of aggressive OSCC [17,22].

We developed a small peptide, ZD2, to selectively target EDB-FN in the tumor microenvironment [19]. Prior work with the ZD2 peptide has demonstrated highly specific binding to the EDB domain of EDB-FN [18–20]. Conjugation of ZD2 to the clinical GBCA gadoteridol yielded a novel EDB-FN-targeting contrast agent, ZD2-Gd(HP-DO3A), that enabled magnetic resonance molecular imaging (MRMI) of the tumor microenvironment [20–21]. Further optimization of ZD2-Gd(HP-DO3A) produced a more efficient targeted contrast agent ZD2-N3-Gd(HP-DO3A) (MT218, Fig. 1a) [15]. MT218 exhibits higher T_1 relaxivity than gadoteridol at 3T, measured at 6.07±1.13 $s^{-1}mM^{-1}$ and 3.20±0.96 $s^{-1}mM^{-1}$, respectively [15,20]. MRMI with the targeted agents differentially enhanced aggressive forms of prostate and triple-negative breast cancers, yet maintained similar stability, clearance kinetics, and safety profile as gadoteridol [16,20–21]. A dosing study demonstrated that MT218 provides comparable, if not greater, contrast enhancement in triple-negative breast cancer even at just 20% of the recommended clinical dose (0.1 mmol/kg) for gadoteridol [15]. Here, we demonstrate the effectiveness of MT218 at reduced dose for diagnostic imaging of EDB-FN-expressing aggressive OSCC using MRMI.

Methods

Cell culture

Human OSCC cell lines CAL27 and SCC4 were purchased from American Type Culture Collection (ATCC, Manassas, VA, USA). OSCC cell line HSC3 was purchased from the Japanese Collection of Research Bioresources Cell Bank (Ibaraki City, Japan) via Sekisui XenoTech (Kansas City, KS, USA). CAL27 and HSC3 were cultured in Dulbecco's Modified Eagle's Medium (DMEM, ATCC) supplemented with 10% fetal bovine serum (FBS, Corning Inc., Corning, NY, USA) and 1% penicillin-streptomycin (PS, Thermo Fisher Scientific, Waltham, MA, USA). SCC4 was cultured in DMEM supplemented with 10% FBS, 1% PS, and 400 ng/mL hydrocortisone (Sigma-Aldrich, St. Louis, MO, USA). Stable green fluorescent protein (GFP)- and firefly luciferase-expressing cell lines were generated by transfecting cells with CMV-Luciferase-2A-GFP lentivirus (Amsbio, Cambridge, MA,

USA) followed by fluorescence-activated cell sorting for GFP expression. CAL27-GFP, SCC4-GFP, and HSC3-GFP cell lines were cultured in the complete medium of the respective parent cell line. All cells were incubated at 37°C in 5% CO_2.

Semi-quantitative real-time PCR

RNA was extracted from cell pellets with an RNeasy Kit (Qiagen, Hilden, Germany). RNA samples were reverse-transcribed into cDNA using a miScript II Reverse Transcription Kit (Qiagen). Semi-quantitative real-time PCR was conducted using a SYBR Green Master Mix (Life Technologies, Carlsbad, CA, USA) according to the manufacturer's recommendations. Relative mRNA levels were calculated using the standard $2^{-\Delta\Delta CT}$ method, using 18S expression as the control gene. cDNA synthesis and qRT-PCR were conducted with the BioRad CFX Connect Real-Time PCR Detection System (Bio-Rad Laboratories, Hercules, CA, USA). Primers purchased from Integrated DNA Technologies (IDT, Coralville, IA, USA) were as follows: 18S Forward: TCAAGAACGAAAGTCGGAGG; 18S Reverse: GGACATCTAAGGGCATCACA; EDB-FN Forward: CCGCTAAACTCTTCCACCATTA, EDB-FN Reverse: AGCCCTGTGACTGTGTAGTA.

Western blot

Cell lysates were prepared from cell pellets with 2× Laemmli sample buffer (Bio-Rad Laboratories) and a protease inhibitor cocktail (Roche Holding AG, Basel, Switzerland) according to the manufacturer's recommendations. Lysates were boiled and centrifuged at 4°C and 15,000 rpm for 15 minutes. The supernatants were collected, and protein concentration was measured via Lowry assay (Bio-Rad Laboratories). Protein extracts (50 μg) were resolved using SDS-PAGE and transferred onto nitrocellulose membranes (Cell Signaling Technology, Danvers, MA, USA) under ice. SDS-PAGE and transfer were conducted using the Bio-Rad Mini PROTEAN Tetra System (Bio-Rad Laboratories). Membranes were blocked with 5% milk, washed, and incubated with anti-EDB-FN (G4, Absolute Antibody, Oxford, UK) and anti-β-actin (CST) primary antibodies (1:2000) in 5% bovine serum albumin (BSA, Sigma-Aldrich) on ice overnight. Membranes were washed and incubated with horseradish peroxidase-conjugated anti-mouse and anti-rabbit IgG secondary antibodies (1:1000, CST) in 5% BSA for 1 hour at room temperature. After washing, membranes were activated with SignalFire Plus ECL Reagent (CST) and imaged with the BioRad Molecular Imager ChemiDoc XRS+ System (Bio-Rad Laboratories).

Spheroid formation and peptide binding studies

Coverslip plates (4-well, Ibidi GmbH, Martinsried, Germany) were coated with Cultrex Basement Membrane Matrix (350 μL, Trevigen, Gaithersburg, MA, USA). For spheroid formation, 2×10^5 OSCC cells were seeded into prepared wells, incubated for 2 days, and photographed with the Moticam T2 camera (Motic, Hong Kong, China). For peptide binding, 1×10^5 cells were seeded into prepared wells and incubated for 2 days. Spheroids were stained with ZD2-Cy5.5 (125 nM), synthesized as previously described, and Hoechst (1:2000 dilution) (Invitrogen, Carlsbad, CA, USA) dyes for 15 minutes, washed 3× with DPBS (Thermo Fisher Scientific), and imaged with confocal laser scanning microscopy using the Olympus FV1000 system (Olympus Life Science, Tokyo, Japan) [20].

Confocal fluorescence images were analyzed using FIJI (https://fiji.sc/). For quantification, images were thresholded to generate ROIs of both stains. For spheroid size, the average size of Hoechst ROIs was calculated. For staining intensity, the average signal intensities of ZD2-Cy5.5 and Hoechst ROIs were calculated, along with the ratio between the average intensities.

Transwell migration and invasion assays

OSCC cells were starved overnight, seeded in serum-free medium (1×10^5 cells) into Transwell ThinCert Inserts (Greiner Bio-One, Kremsmünster, Austria) coated with (invasion) or without (migration) 100 μL of 1.0 mg/mL Matrigel (Corning), and placed above complete medium. Inserts for migration and invasion were incubated for 1 and 2 days, respectively. Cells on the underside of inserts were fixed with 10% formalin, stained with 0.1% crystal violet, and imaged with the Moticam T2 camera.

Animal models

Animal experiments were performed under an animal protocol approved by the Institutional Animal Care and Use Committee (IACUC) at Case Western Reserve University (CWRU, Cleveland, OH, USA). Female 4-week-old athymic nude mice purchased from the Jackson Laboratory (Bar Harbor, ME, USA) were housed in the Animal Core Facility at CWRU. Anesthetized mice were subcutaneously inoculated in the right flank with 4×10^6 GFP/luciferase-expressing OSCC cells (n=5 per cell line) in 100 μL of a 1:1 mixture of Matrigel HC (Corning) and DPBS. Tumor size was monitored with caliper measurements. After 4 weeks of growth, mice bearing tumors that were sufficiently large (>100 mm^3) were used for MRI experiments.

MR molecular imaging

MRI experiments were performed with a 3T MRS-3000 system (MR Solutions, Surrey, UK). The T_1 values of MT218 and gadoteridol solutions at 3T were measured using an inversion recovery FLASH sequence. The r_1 relaxivities were calculated from the slopes of $1/T_1$ versus gadolinium concentration [20].

For animal experiments, tumor-bearing mice were anesthetized with isoflurane and maintained at a respiration rate between 70–90 breaths per minute and a temperature between 37–38 °C. The tail vein was cannulized with a catheter for intravenous administration of the contrast agent. Mice were imaged before and at 10, 20, 30, and 40 minutes post-injection of the targeted contrast agent, MT218 (Molecular Theranostics, LLC, Cleveland, OH, USA), at a dose of 0.04 mmol/kg using a T_1-weighted fast spin-echo axial sequence with respiratory gating (T_R=305 ms, T_E=11 ms, FOV=40×40 mm, slice thickness=1 mm, number of slices=15, N_{av}=2, matrix=256×248). This protocol was repeated on the same mice 2 days later using the untargeted clinical agent gadoteridol at the clinical dose of 0.10 mmol/kg. For the blocking study with the SCC4 cohort, the above protocol was repeated using a 10x excess free ZD2 peptide co-injection with 0.04 mmol/kg MT218.

Images were exported in DICOM format and analyzed using FIJI. Contrast-to-noise ratio (CNR) for each time point was calculated as the difference between the mean tumor

intensity and the mean muscle intensity, divided by the standard deviation of noise (Supp. Fig. 1).

Xenograft histological analysis

Mice were euthanized according to IACUC guidelines. Xenograft tumors were fixed in 10% formalin, paraffin-embedded, and sectioned in 5 μm slices onto coverslip slides. Tissues underwent routine H&E staining for tissue morphology and immunohistochemical staining using the EDB-FN-specific antibody, G4, at a 1:100 dilution. Antigen retrieval was performed prior to immunohistochemistry using citrate buffer in a pressure cooker at 125 °C for 30 seconds. Tissue preparation and staining was conducted by the Tissue Resources Core at CWRU.

Human tissue procurement and histological analysis

Human normal tongue and OSCC specimens were obtained in 5 μm slices on coverslip slides from the Human Tissue Procurement Facility at CWRU. Tissue samples were fully deidentified according to a non-human subject research protocol approved by the Institutional Review Board at CWRU. Immunohistochemical staining for EDB-FN was conducted by the Tissue Resources Core in the same manner as the xenograft histological analysis.

Statistical analysis

All experiments were independently replicated three times unless otherwise stated. Statistical significance between two groups was calculated using an unpaired T-Test. Statistical significance between more than two groups with one and two independent variables was calculated using one-way and two-way ANOVA, respectively, followed by Fisher's least significant difference post-hoc tests. P-values less than 0.05 were considered statistically significant. All data is presented as mean ± standard error.

Results

EDB-FN expression in human tissues

To evaluate the clinical relevance of targeting EDB-FN for OSCC in patients, EDB-FN expression in human tissue samples was evaluated by immunohistochemistry with an EDB-FN specific G4 monoclonal antibody. While normal tongue tissue showed weak punctate staining for EDB-FN primarily in the stroma, untreated primary OSCC and metastatic specimens demonstrated strong staining of malignant epithelial cells and surrounding stroma (Fig. 1b–d). These results are consistent with previous reported results of EDB-FN expression in human OSCC using the BC-1 monoclocal antibody [17,22]. Interestingly, tumors excised after neoadjuvant treatment exhibited reduced staining than untreated tumors, potentially suggesting EDB-FN downregulation after the treatment (Fig. 1e). These results underscore the potential for exploring EDB-FN as an oncoprotein target for molecular imaging of both primary and metastatic OSCC.

Characterization of OSCC cell lines

Three human OSCC cell lines were used to assess the effectiveness of MRMI of EDB-FN for diagnostic imaging of OSCC. CAL27 and SCC4 were isolated from the primary sites in the tongue before and after treatment, respectively [23–24]. CAL27 maintains an epithelial, cobblestone-like layout of cells, while SCC4 is replete with polyploid giant cells (Fig. 2a). Interestingly, polyploid giant cells are often indicative of morphological changes due to treatment stress and have been associated with tumor recurrence, drug resistance, and heterogeneity [25–27]. HSC3, on the other hand, was isolated from a cervical lymph node metastasis and has high metastatic potential among the tumor models [28].

When cultured on basement membrane extract for spheroid formation, CAL27 forms many small punctate spheroids while HSC3 and SCC4 form large dense networks that spread throughout the gel (Fig. 2a). Further, transwell assays were performed with and without Matrigel coating to characterize the invasive and migratory capacity of the cell lines, respectively. In both experiments, CAL27 showed limited ability to migrate or invade, while HSC3 and SCC4 showed substantial invasive potential (Fig. 2b). These data demonstrate that HSC3 and SCC4, derived from a metastatic site and post-treatment primary tumor, respectively, represent aggressive, high-risk OSCC, while CAL27, derived from a pre-treatment primary tumor, represents a less aggressive, low-risk OSCC.

EDB-FN is a targetable oncoprotein associated with high-risk OSCC

EDB-FN expression was analyzed to determine its correlation with aggressiveness in OSCC. qRT-PCR analysis showed significantly upregulated EDB-FN mRNA in invasive HSC3 (21-fold) and SCC4 (234-fold) cells relative to non-invasive CAL27 (Fig. 3a). Further, SCC4 exhibited 11-fold higher upregulated EDB-FN mRNA than HSC3. This result was corroborated on the protein level by western blotting, demonstrating that EDB-FN is differentially expressed and upregulated in invasive OSCC (Fig. 3b).

Spheroids were stained with an EDB-FN-specific fluorescence probe ZD2-Cy5.5 to assess targeting EDB-FN for molecular imaging of OSCC. Aggressive HSC3 and SCC4 cells formed larger spheroids with notably stronger staining of ZD2-Cy5.5 compared to CAL27 (Fig. 3c–d). Quantification of the staining intensity also revealed approximately 2-fold stronger staining of SCC4 than HSC3, in agreement with the EDB-FN expression analysis (Fig. 3e). This data demonstrates that the ZD2 peptide can effectively target differentially expressed EDB-FN for molecular imaging of OSCC.

MT218 differentially enhances EDB-FN-expressing OSCC in MRMI

The effectiveness of MT218 for MRMI of EDB-FN in OSCC at a subclinical dose in correlation with tumor aggressiveness was determined in mouse flank xenograft models, using the clinical agent gadoteridol as an untargeted control. Low-risk, low-EDB-FN CAL27 tumors exhibited moderate enhancement with MT218 at 0.04 mmol/kg that washed out by 40 minutes post-injection. Enhancement with gadoteridol at 0.10 mmol/kg in CAL27 tumors appeared slightly greater than MT218 because of its high dose (Fig. 4a). High-risk, moderate-EDB-FN HSC3 tumors showed strong enhancement with MT218 at 10 minutes post-injection, which reduced significantly by 40 minutes. Enhancement with gadoteridol in

HSC3 tumors appeared slightly less than, but generally comparable to, MT218 despite the dose reduction of the latter (Fig. 4b). High-risk, high-EDB-FN SCC4 tumors exhibited substantial enhancement with MT218 at all the time-points. Enhancement with gadoteridol in SCC4 tumors was much weaker than MT218 (Fig. 4c). In addition, blocking MT218 binding with free ZD2 peptide abrogated the increased enhancement observed with unblocked MT218 (Supp. Fig. 2a). These images suggest that MT218 selectively and differentially enhances high-risk OSCC tumors at a subclinical dose in accordance with their EDB-FN expression, a property unachievable with the clinical contrast agent.

Semi-quantitative analysis of contrast enhancement

Contrast-to-noise ratios (CNR) in the tumors were calculated for semi-quantitative analysis of tumor enhancement with MT218 and gadoteridol. MT218 differentially enhanced the three tumor models at all the time-points in accordance with their EDB-FN expression, while gadoteridol showed no differential enhancement at any time point (Fig. 5a–b). Low-risk, low-EDB-FN CAL27 tumors showed significantly lower enhancement with MT218 than gadoteridol except at 10 and 40 minutes post-injection (Fig. 5c). High-risk, moderate-EDB-FN HSC3 tumors exhibited significantly higher enhancement with MT218 than gadoteridol at 10 minutes post-injection and trended higher until 40 minutes post-injection (Fig. 5d). High-risk, high-EDB-FN SCC4 tumors exhibited significantly higher CNR enhancement with MT218 than gadoteridol at all the time-points (Fig. 5e). When blocked with free ZD2 peptide, SCC4 tumors exhibited similar CNR enhancement to gadoteridol, demonstrating the binding of MT218 to improve enhancement (Supp. Fig. 2b).

The average maximum CNR enhancement between MT218 and gadoteridol was borderline significantly lower for CAL27 (CNR_{MT218}=1.80±0.17, CNR_{gad}=2.27±0.18, p=0.0957), borderline significantly higher for HSC3 (CNR_{MT218}=2.61±0.17, CNR_{gad}=2.18±0.07, p=0.0639), and significantly higher for SCC4 (CNR_{MT218}=3.81±0.25, CNR_{gad}=2.57±0.28, p=0.0170) (Fig. 5f–h). The average maximum CNR enhancement with MT218 was significantly different between the three tumor models in accordance with their EDB-FN expression, while there were no significant differences with gadoteridol (Fig. 5i). When blocked with free ZD2 peptide, the average maximum CNR enhancement with MT218 was slightly lower than gadoteridol ($CNR_{MT218,blocked}$=2.29±0.28, CNR_{gad}=2.66±0.38, p=0.4714) and was substantially lower than that of unblocked MT218 ($CNR_{MT218,blocked}$=2.29±0.28, $CNR_{MT218,unblocked}$=3.81±0.25, p=0.0105) (Supp. Fig. 2c–e). These data validate the unique ability of MT218 to selectively and differentially enhance EDB-FN-expressing high-risk OSCC tumors in MRMI at a subclinical dose.

Histological analysis of xenograft tumors

The tumors were excised post-imaging for histological and immunohistochemical analysis. Low-risk, moderately-differentiated CAL27 tumors exhibited weak EDB-FN staining in epithelial regions, with stromal staining increasing near the tumor boundary (Fig. 6). High-risk, poorly-differentiated HSC3 tumors exhibited stronger EDB-FN staining than corresponding regions in CAL27 tumors, with little stroma for interpretation (Fig. 6). High-risk, well-differentiated SCC4 tumors showed membranous staining for EDB-FN within and around epithelial regions that was the strongest of the three tumor models, while the large

keratinizing stromal regions showed little staining (Fig. 6). The EDB-FN staining intensity of the epithelial tumor regions was in agreement with the *in vitro* EDB-FN expression analysis and the CNR analysis of MRMI data, suggesting that contrast enhancement in MRMI with MT218 of OSCC increases with increasing EDB-FN expression and can be used for differentiating aggressive from non-aggressive OSCC.

Discussion

MRI is commonly used for the diagnosis of OSCC, providing unrivaled soft tissue contrast and high resolution that allows delineation of primary and metastatic disease and assists treatment planning [9–11]. Additionally, MRI does not expose patients to harmful radiation, and GBCAs are typically less nephrotoxic at clinical doses than iodine-based CT contrast agents [29]. In this study, MRMI with the targeted contrast agent MT218 provided robust enhancement in high-risk OSCC tumors at 0.04 mmol/kg, just 40% of the clinical dose of 0.10 mmol/kg. Similar results with MT218 were observed in aggressive triple-negative breast cancer at a dose as low as 20% of the clinical dose [16]. The increased enhancement is primarily derived from the selective binding of MT218 to EDB-FN in the tumor ECM, allowing temporary accumulation and retention of MT218 in the tumor [20–21]. Biodistribution studies in prior work with MT218 has demonstrated similar clearance kinetics from the blood and off-target organs as that of gadoteridol [16,20]. Effective MRMI of aggressive tumors with MT218 at subclinical doses would significantly improve the clinical safety of GBCAs, mitigating potential dose-dependent side effects associated with gadolinium administration.

Lymph node metastasis is one of the most important prognostic indicators for OSCC, and occult metastasis occurs in 20–40% of patients with a clinically and radiologically negative neck [30–32]. Standard practice to identify regional metastases includes physical examination and diagnostic imaging, but many metastases are regularly overlooked or unidentifiable due to their very small size [9,33]. While elective neck dissection removes potentially affected lymph nodes, subsequent histological examination reveals many unnecessary dissections [32,35–36]. We previously demonstrated that highly specific targeted GBCAs enable detection of micrometastatic breast cancer [36]. We also observed strong EDB-FN expression in metastatic OSCC specimens and cells, in agreement with previous studies [17,22]. Future studies will explore MRMI with the EDB-FN-targeting contrast agent MT218 as a promising new strategy for more accurate detection and diagnosis of OSCC metastases to improve precision management and personalized treatment of the disease.

Anti-cancer treatments can directly affect ECM protein expression, yielding a dynamic ECM that mediates tumor initiation, progression, and therapeutic efficacy [14,37–39]. Chemoresistance is regularly associated with increased AKT signaling and downstream fibronectin and EDB-FN expression [13–14,18]. We observed reduced EDB-FN expression in neoadjuvant OSCC specimens, but increased expression in OSCC cells derived from a patient who had undergone extensive long-term treatment. In addition, more than 20% of head and neck squamous cell carcinoma patients experience locoregional tumor recurrence after surgical resection, after which the 5-year survival rate falls to 30% [40–41]. Future

studies will explore the potential of MRMI with MT218 to associate and visualize treatment response with changes in EDB-FN expression. Such information would provide physicians insight into the acquisition of high-risk features like drug resistance to improve timely and personalized treatment, as well as monitor for tumor recurrence post-resection for precision management of the disease.

While the MRI technique used in the study is semiquantitative, incorporating CNR analysis, the use of MT218 in quantitative MRI techniques, e.g. MR fingerprinting, would provide fast, accurate and robust measurements of proton density, T_1, and T_2 maps. Mapping the changes in T_1 values due to the contrast agent would allow for measurement of the concentration of the agent within the tumor [42]. As MT218 binds with EDB-FN in the tumor, this offers a means of EDB-FN measurement, provided proper calibration. Future studies will explore the potential of measuring EDB-FN expression with MT218 in quantitative MRI and its ability to discriminate aggressive OSCC tumors based upon expression measurements.

This preclinical study has several other limitations. The role of EDB-FN in cancer biology is largely unclear and needs further investigation at the molecular, preclinical and clinical levels. Further investigations are also needed for comprehensive evaluation of EDB-FN as a viable biomarker for aggressive OSCC. Future work will focus on the validation of EDB-FN as an imageable biomarker of OSCC and clinical translation of MRMI with MT218 for precision imaging of OSCC.

Conclusions

We showed the preliminary correlation between EDB-FN expression and aggressiveness of human OSCC cells, tumors models, and patient specimens. MRMI of EDB-FN with MT218 provided substantial and differential contrast enhancement in OSCC tumor models in correlation with their inherent EDB-FN expression and aggressiveness at a subclinical dose. Gadoteridol meanwhile provided modest undifferentiated enhancement at the clinical dose. The results indicate that MRMI with the EDB-FN-targeting contrast agent MT218 has the potential to provide accurate diagnosis, risk assessment, delineation, and therapeutic efficacy monitoring in clinical management of OSCC.

Supplementary Material

Refer to Web version on PubMed Central for supplementary material.

Acknowledgements

This work was supported in part by the National Institutes of Health grants R01 CA194518, R01211762 and R44 CA199826, and by the Tissue Resources Core Facility of the Comprehensive Cancer Center of Case Western Reserve University and University Hospitals of Cleveland (P30 CA43703). ZR Lu is M. Frank Rudy and Margaret Domiter Rudy Professor of Biomedical Engineering. We also wish to thank Adam Kresak and Jenifer Mikulan at the Case Comprehensive Cancer Center for their technical assistance on the project.

References

1. Rivera C (2015) Essentials of oral cancer. Int J Clin Exp Pathol 8:11884–11894.

2. Chen SW, Zhang Q, Guo ZM, et al. (2018) Trends in clinical features and survival of oral cavity cancer: fifty years of experience with 3,362 consecutive cases from a single institution. Cancer Manag Res 10:4523–4535. [PubMed: 30349385]

3. Sarode GS, Sarode SC, Maniyar N, et al. (2019) Recent trends in predictive biomarkers for determining malignant potential of oral potentially malignant disorders. Oncol Rev 13:424. [PubMed: 31565195]

4. Seoane-Romero JM, Vázquez-Mahía I, Seoane J, et al. (2012) Factors related to late stage diagnosis of oral squamous cell carcinoma. Med Oral Patol Oral Cir Bucal 17:35–40.

5. Brandwein-Gensler M, Teixeira MS, Lewis CM, et al. (2005) Oral squamous cell carcinoma: histologic risk assessment, but not margin status, is strongly predictive of local disease-free and overall survival. Am J Surg Pathol 29:167–178. [PubMed: 15644773]

6. Adelstein D, Gillison ML, Pfister DG, et al. (2017) NCCN Guidelines Insights: Head and Neck Cancers, Version 2.2017. J Natl Compr Canc Netw 15:761–770. [PubMed: 28596256]

7. Cho JH, Lee YS, Sun DI, et al. (2016) Prognostic impact of lymph node micrometastasis in oral and oropharyngeal squamous cell carcinoma. Head Neck 38 Suppl 1:E1777–1782.

8. Lingen MW, Tampi MP, Urguhart O, et al. (2017) Adjuncts for the evaluation of potentially malignant disorders in the oral cavity: diagnostic test accuracy systematic review and meta-analysis-a report of the American Dental Association. J Am Dent Assoc 148:797–813. [PubMed: 29080605]

9. Pałasz P, Adamski Ł, Górska-Chrzastek M, Starzyńska A, Studniarek M (2017) Contemporary diagnostic imaging of oral squamous cell carcinoma – a review of literature. Pol J Radiol 82:193–202. [PubMed: 28439324]

10. Seeburg DP, Baer AH, Aygun N (2018) Imaging of patients with head and neck cancer: from staging to surveillance. Oral Maxillofac Surg Clin North Am 30:421–433. [PubMed: 30143307]

11. Abraham J (2015) Imaging for head and neck cancer. Surg Oncol Clin N Am 24:455–471. [PubMed: 25979394]

12. Zhou Z, Lu ZR (2013) Gadolinium-based contrast agents for MR cancer imaging. Wiley Interdiscip Rev Nanomed Nanobiotechnol 5:1–18. [PubMed: 23047730]

13. Zhou Z, Lu ZR (2017) Molecular imaging of the tumor microenvironment. Adv Drug Deliv Rev 113:24–48. [PubMed: 27497513]

14. Han Z, Lu ZR (2017) Targeting fibronectin for cancer imaging and therapy. J Mater Chem B 5:639–654. [PubMed: 29270293]

15. Ayat NR, Qin JC, Cheng H, et al. (2018) Optimization of ZD2 peptide targeted Gd(HP-DO3A) for detection and risk-stratification of prostate cancer with MRI. ACS Med Chem Lett 9:730–735. [PubMed: 30034609]

16. Ayat NR, Vaidya A, Yeung GA, et al. (2019) Effective MR molecular imaging of triple negative breast cancer with an EDB-fibronectin-specific contrast agent at reduced doses. Front Oncol 9:1351. [PubMed: 31850230]

17. Birchler MT, Milisavlijevic D, Pfaltz M, et al. (2003) Expression of the extra domain B of fibronectin, a marker of angiogenesis, in head and neck tumors. Laryngoscope 113:1231–1237. [PubMed: 12838025]

18. Vaidya AM, Wang H, Qian V, Lu ZR (2019) Extradomain-B fibronectin is a molecular marker of invasive breast cancer cells. bioRxivorg doi: 10.1101/743500.

19. Han Z, Zhou Z, Shi X, et al. (2015) EDB fibronectin specific peptide for prostate cancer targeting. Bioconjug Chem 26:830–838. [PubMed: 25848940]

20. Han Z, Li Y, Roelle S, et al. (2017) Targeted contrast agent specific to an oncoprotein in tumor microenvironment with the potential for detection and risk stratification of prostate cancer with MRI. Bioconjug Chem 28:1031–1040. [PubMed: 28201871]

21. Han Z, Cheng H, Parvani JG, Zhou Z, Lu ZR (2018) Magnetic resonance molecular imaging of metastatic breast cancer by targeting extradomain-B fibronectin in the tumor microenvironment. Magn Reson Med 79:3135–3143. [PubMed: 29082597]

22. Mandel U, Gaggero B, Reibel J, et al. (1994) Oncofetal fibronectins in oral carcinomas: correlation of two different types. APMIS 102:695–702. [PubMed: 7946273]

23. Gioanni J, Fischel JL, Lambert JC, et al. (1988) Two new human tumor cell lines derived from squamous cell carcinomas of the tongue: establishment, characterization and response to cytotoxic treatment. Eur J Cancer Clin Oncol 24:1445–1455. [PubMed: 3181269]
24. Rheinwald JG, Beckett MA (1981) Tumorigenic keratinocyte lines requiring anchorage and fibroblast support cultured from human squamous cell carcinomas. Cancer Res 41:1657–1663. [PubMed: 7214336]
25. Mirzayans R, Andrais B, Murray D (2018) Roles of polyploid/multinucleated giant cancer cells in metastasis and disease relapse following anticancer treatment. Cancers (Basel) 10:118.
26. Amend SR, Torga G, Lin KC, et al. (2019) Polyploid giant cancer cells: unrecognized actuators of tumorigenesis, metastasis, and resistance. Prostate 79:1489–1497. [PubMed: 31376205]
27. Bharadwaj D, Mandal M (2019) Senescence in polyploid giant cancer cells: A road that leadsto chemoresistance. Cytokine Growth Factor Rev 52:68–75. [PubMed: 31780423]
28. Momose F, Araida T, Negishi A, et al. (1989) Variant sublines with different metastatic potentials selected in nude mice from human oral squamous cell carcinomas. J Oral Pathol Med 18:391–395. [PubMed: 2585303]
29. Prince MR, Arnoldus C, Frisoli JK (1996) Nephrotoxicity of high-dose gadolinium compared with iodinated contrast. J Magn Reson Imaging 6:162–166. [PubMed: 8851422]
30. Kapoor C, Vaidya S, Wadhwan V, Malik S (2015) Lymph node metastasis: a bearing on prognosis in squamous cell carcinoma. Indian J Cancer 52:417–424. [PubMed: 26905157]
31. Li Y, Liu K, Ke Y, et al. (2019) Risk factors analysis of pathologically confirmed cervical lymph nodes metastasis in oral squamous cell carcinoma patients with clinically negative cervical lymph node: results from a cancer center of central China. J Cancer 10:3062–3069. [PubMed: 31281484]
32. Zbären P, Nuyens M, Caversaccio M, Stauffer E (2006) Elective neck dissection for carcinomas of the oral cavity: occult metastases, neck recurrences, and adjuvant treatment of pathologically positive necks. Am J Surg 191:756–760. [PubMed: 16720144]
33. Dhawan I, Sandhu SV, Bhandari R, et al. (2016) Detection of cervical lymph node micrometastasis and isolated tumor cells in oral squamous cell carcinoma using immunohistochemistry and serial sectioning. J Oral Maxillofac Pathol 20:436–444. [PubMed: 27721609]
34. de Bree R, Takes RP, Shah JP, et al. (2019) Elective neck dissection in oral squamous cell carcinoma: past, present and future. Oral Oncol 90:87–93. [PubMed: 30846183]
35. D'Cruz AK, Vaish R, Kapre N, et al. (2015) Elective versus therapeutic neck dissection in node-negative oral cancer. N Engl J Med 373:521–529. [PubMed: 26027881]
36. Zhou Z, Qutaish M, Han Z (2015) MRI detection of breast cancer micrometastases with a fibronectin-targeting contrast agent. Nat Commun 6:7984. [PubMed: 26264658]
37. Harisi R, Jeney A (2015) Extracellular matrix as target for antitumor therapy. Onco Targets Ther 8:1387–1398. [PubMed: 26089687]
38. Roma-Rodrigues C, Mendes R, Baptista PV, Fernandes AR (2019) Targeting tumor microenvironment for cancer therapy. Int J Mol Sci 20:840.
39. Raavé R, van Kuppevelt TH, Daamen WF (2018) Chemotherapeutic drug delivery by tumoral extracellular matrix targeting. J Control Release 274:1–8. [PubMed: 29382546]
40. Chang JH, Wu CC, Yuan KSP, Wu ATH, Wu SY (2017) Locoregionally recurrent head and neck squamous cell carcinoma: incidence, survival, prognostic factors, and treatment outcomes. Oncotarget 8:55600–55612.
41. Brands MT, Smeekens EAJ, Takes RP (2019) Time patterns of recurrence and second primary tumors in a large cohort of patients treated for oral cavity cancer. Cancer Med 8:5810–5819. [PubMed: 31400079]
42. Horshtuis K, Nederveen AJ, de Feiter MW, et al. (2009) Mapping of T_1-values and gadolinium-concentrations in MRI as indicator of disease activity in Luminal Crohn's Disease: a feasibility study. J Magn Reson Imaging 29:488–493. [PubMed: 19161209]

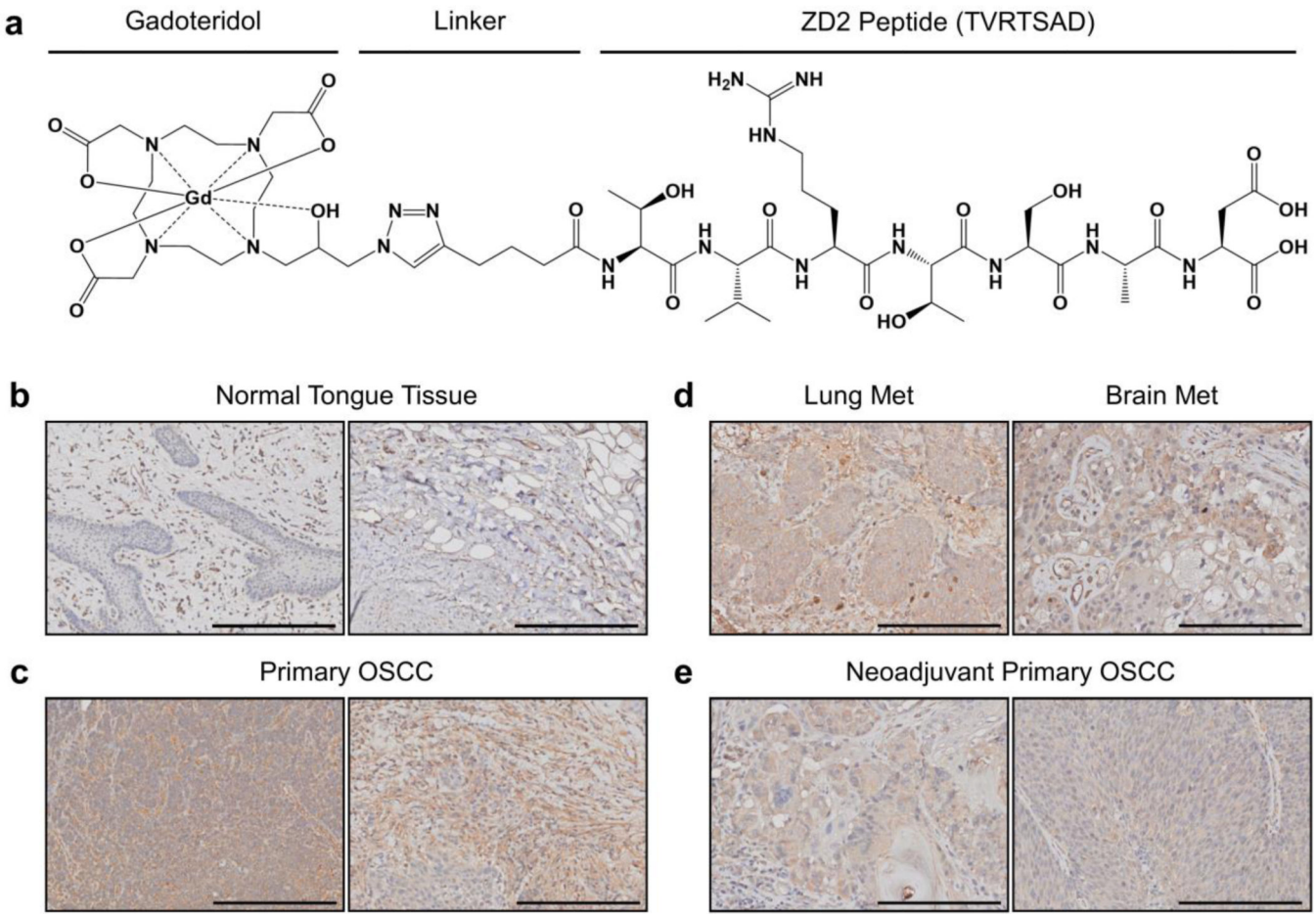

Fig. 1.

(**a**) Molecular structure of the EDB-FN-specific contrast agent MT218. (**b-d**) Immunohistochemical staining of EDB-FN in human tissues with the EDB-FN-specific G4 antibody was (**b**) weak in normal tongue specimens (n=3), (**c**) strong in untreated primary OSCC specimens (n=7), (**d**) strong in OSCC metastatic specimens (n=2), and (**e**) moderate in neoadjuvant primary OSCC specimens (n=3). Scale bars in all panels: 200 μm.

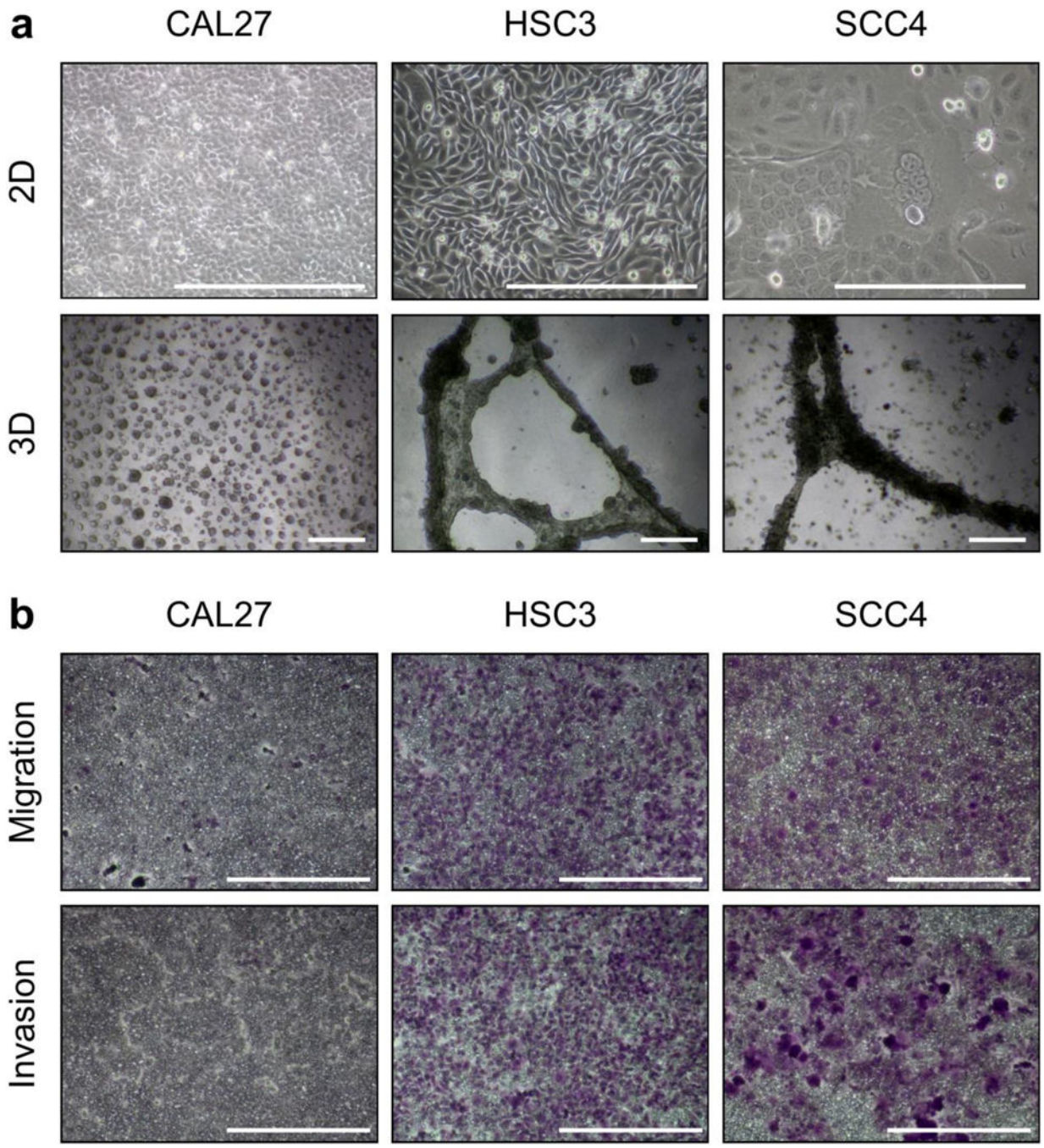

Fig. 2.

(**a**) Cells grown in 2D and 3D culture (n=3) showed high-risk features in HSC3 and SCC4 cells, but not CAL27 cells. (**b**) Transwell migration and invasion assays (n=3) demonstrated high invasive potential of HSC3 and SCC4 cells, but not CAL27 cells. Scale bars in all panels: 400 μm.

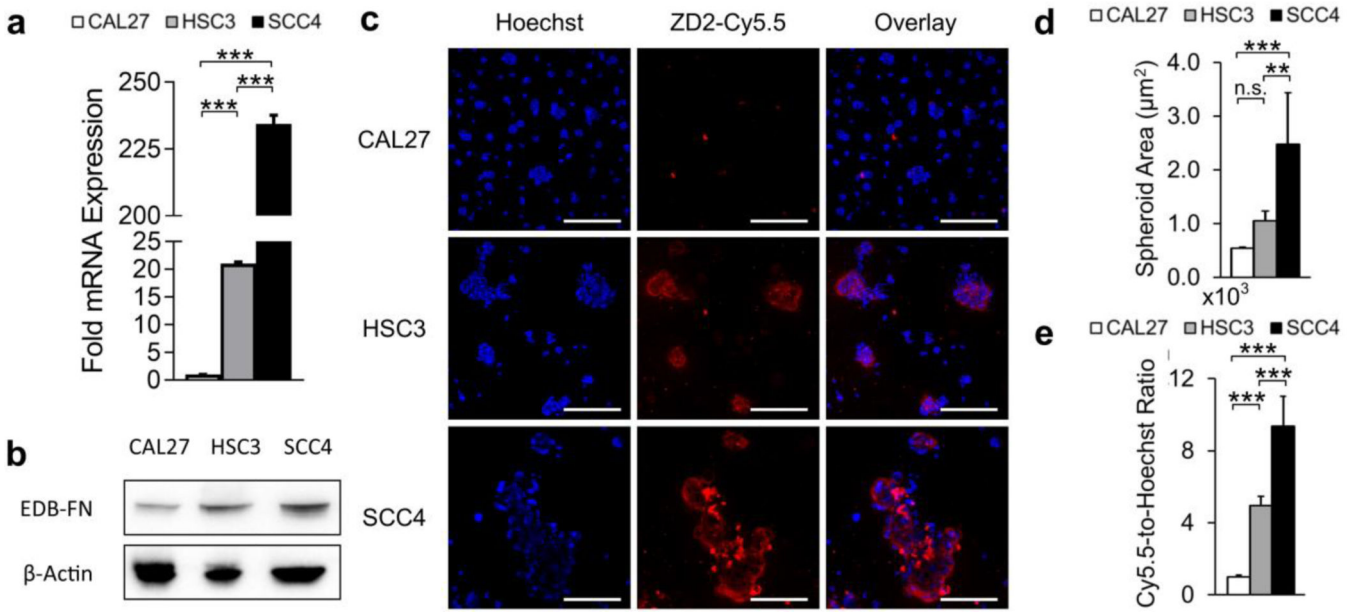

Fig. 3.

(**a**) qRT-PCR mRNA analysis (n=3) and (**b**) western blot protein analysis (n=3) revealed differential and upregulated expression of EDB-FN in aggressive HSC3 and SCC4 cells. (**c**) Peptide binding study of spheroids with EDB-FN-specific ZD2-Cy5.5 (n=3) showed strong staining in HSC3 and SCC4 spheroids, but not CAL27 spheroids. Quantification of confocal images revealed (**d**) larger spheroids and (**e**) stronger ZD2-Cy5.5 staining in HSC3 and SCC4 spheroids in accordance with their EDB-FN expression levels. Data was analyzed with One-Way ANOVA and Fisher's least significant difference post-hoc tests (*, $p<0.05$; **, $p<0.01$; ***, $p<0.001$; n.s., $p>0.05$). Scale bars for confocal images: 200 μm.

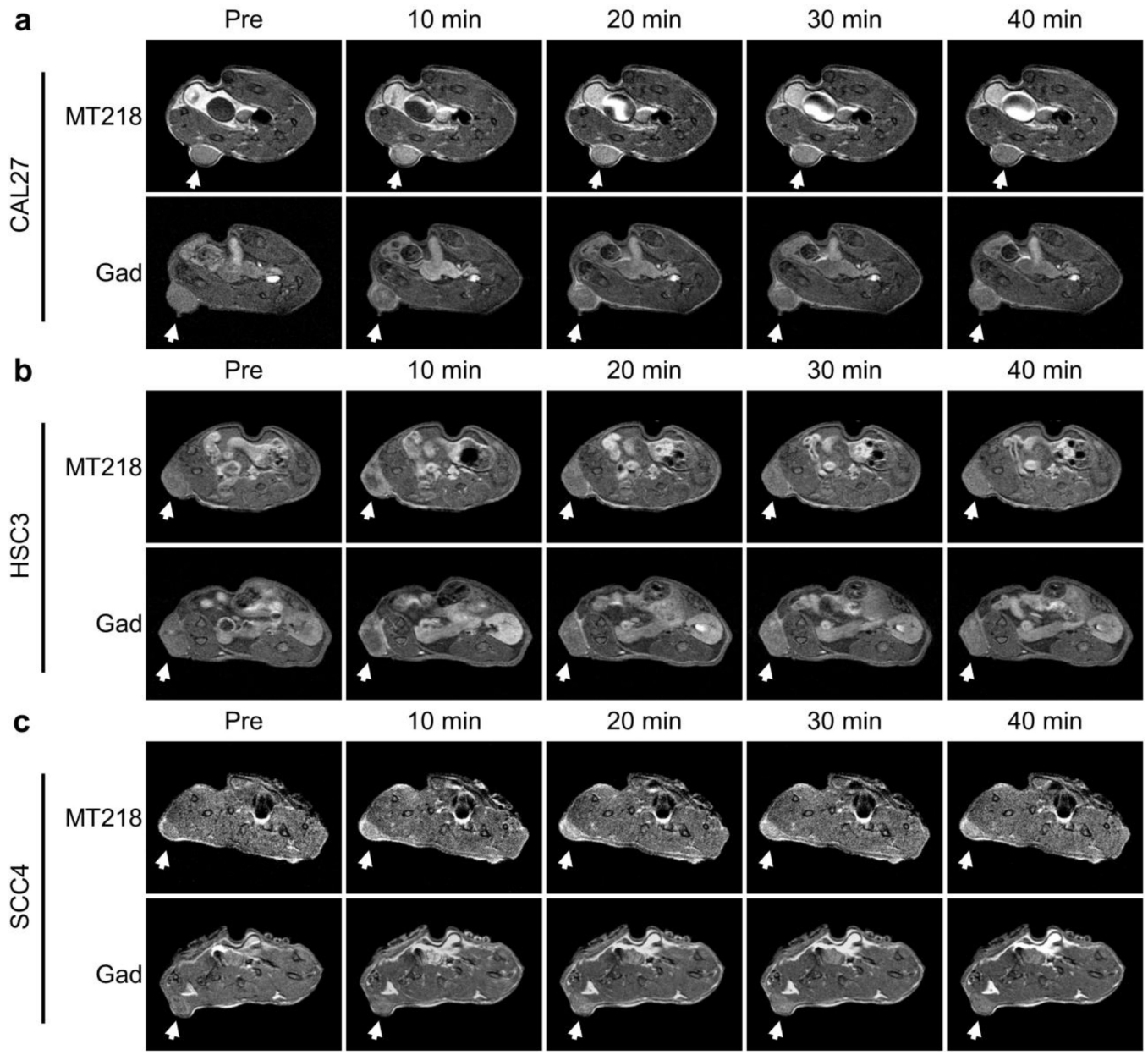

Fig. 4.

(**a**) CAL27 tumors (n=5 for pre, 10, 20, and 30 minutes, n=4 for 40 minutes) showed slightly less enhancement with MT218 than gadoteridol. (**b**) HSC3 tumors (n=4) showed slightly more enhancement with MT218 than gadoteridol. (**c**) SCC4 tumors (n=4) showed substantially more enhancement with MT218 than gadoteridol. MT218 and gadoteridol were used at doses of 0.04 mmol/kg and 0.10 mmol/kg, respectively.

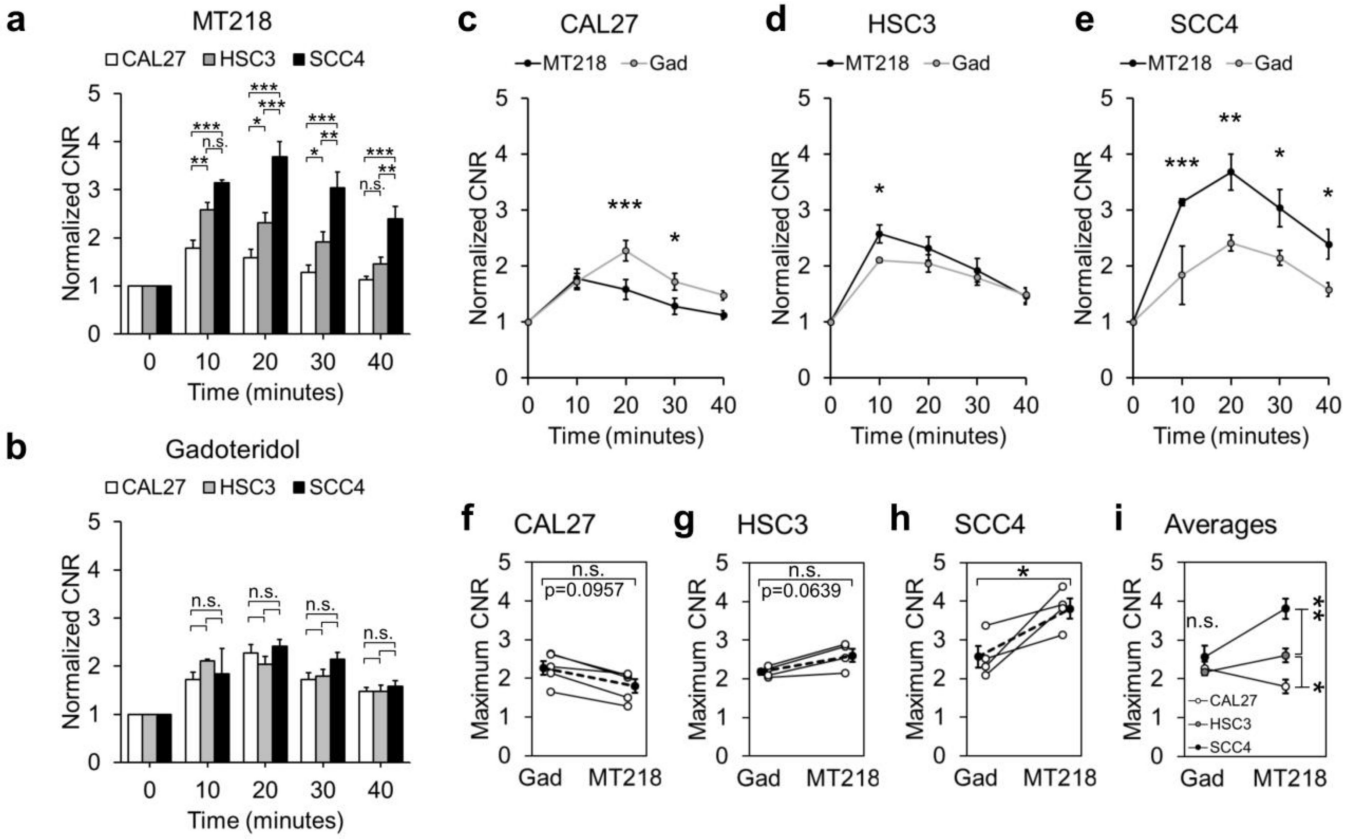

Fig. 5.

CNR analysis of contrast-enhanced tumors revealed (**a**) significant differential enhancement between CAL27, HSC3, and SCC4 tumors with MT218 in accordance with their EDB-FN expression, while (**b**) gadoteridol showed no difference in enhancement between the three models. Enhancement with MT218 was (**c**) generally lower than gadoteridol in CAL27 tumors, (**d**) generally higher than gadoteridol in HSC3 tumors, and (**e**) substantially higher than gadoteridol in SCC4 tumors. Maximum CNR enhancement in subjects with MT218 was (**f**) borderline lower than gadoteridol in CAL27 tumors (p=0.0957), (**g**) borderline higher than gadoteridol in HSC3 tumors (p=0.0639), and (**h**) significantly higher than gadoteridol in SCC4 tumors. (**f-h**) Open dots connected with a solid line represent matched mouse-by-mouse data, and solid dots connected with a dotted line represent cohort averages. (**i**) Average maximum CNR enhancement was significantly different between the three tumor models in accordance with their EDB-FN expression with MT218, but not with gadoteridol. Data was analyzed with Two-Way ANOVA and Fisher's least significant difference post-hoc test (**a-e,i**) and unpaired T-tests (**f-h**) (*, $p<0.05$; **, $p<0.01$; ***, $p<0.001$; n.s., $p>0.05$).

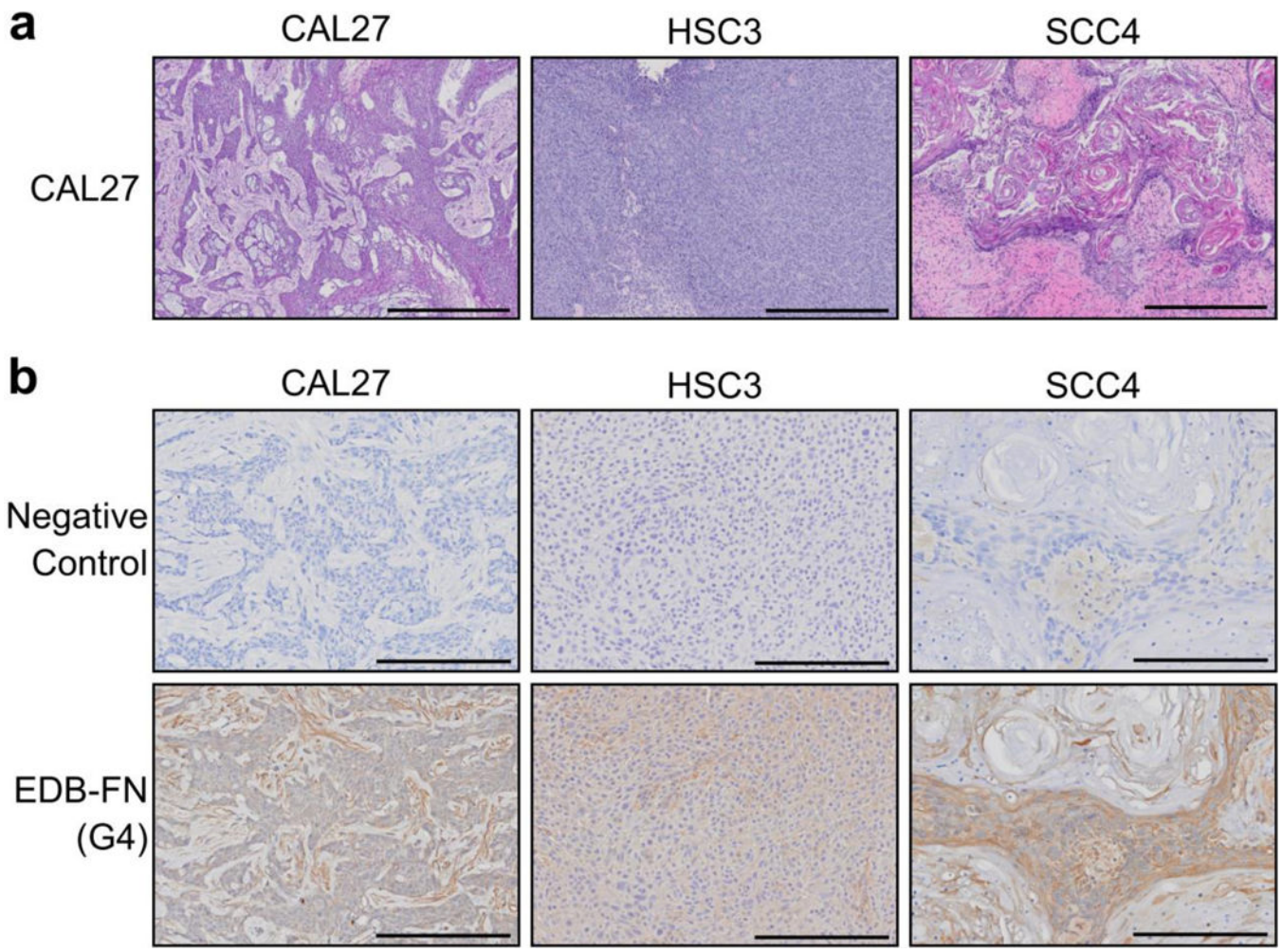

Fig. 6.

(**a**) H&E staining of OSCC xenografts (n=3) showed various morphological features and stages of differentiation. (**b**) Immunohistochemistry for EDB-FN with the EDB-FN-specific G4 antibody (n=3) showed weak, moderate and strong staining in the epithelial regions of CAL27, HSC3, and SCC4 tumors, respectively, with little nonspecific staining. Scale bars: 600μm for H&E images, 200μm for immunohistochemistry images.